Journal of
Applied Crystallography
ISSN 0021-8898

Received 24 August 2010
Accepted 23 November 2010

Effect of necking on Czochralski-grown LiF crystals and its influence on crystalline perfection and the correlated physical properties

G. Bhagavannarayana,* S. K. Kushwaha, Mohd. Shakir and K. K. Maurya

National Physical Laboratory, Council of Scientific and Industrial Research, New Delhi, 110012, India. Correspondence e-mail: bhagavan@mail.nplindia.ernet.in

A bulk single crystal of lithium fluoride (LiF) was grown using an in-house-developed Czochralski crystal puller. The effect of necking on crystalline perfection, which in turn was found to influence the optical and dielectric properties, was studied. The crystalline perfection of the grown crystal was assessed along the length of the boule using high-resolution X-ray diffraction (HRXRD), and it was found that the grain boundaries that were present in the seed crystal were stopped gradually from propagating into the bulk crystal by necking. The UV–vis transparency of the crystal region having best crystalline perfection was found to be higher. Photoluminescence (PL) spectra revealed that a crystal region that was found to contain vacancy (point) defects by HRXRD yielded the maximum PL intensity because of color centers at the vacancies. The dielectric properties were also studied over a wide range of frequency.

1. Introduction

Lithium fluoride (LiF) is one of the best materials for dosimeter applications (Salah & Rupasov, 2007). It also has a higher permittivity than other fluorides – close to that of sapphire and magnesium oxide – for which reason LiF may be used as a substrate for superconducting thin films. The room-temperature color centers in LiF are useful for tunable laser applications in the near IR (Dergachev & Mirov, 1998; Basiev *et al.*, 1997). Single crystals of LiF are highly transparent to the UV–optical spectrum, and therefore it is a suitable candidate for optical windows, prisms and lenses in the UV to IR region (http://www.crystran.co.uk/lithium-fluoride-lif.htm). LiF can also be used in X-ray monochromator plates because its lattice spacing is appropriate for an analyzer crystal (http://www.almazoptics.com/LiF.htm).

Crystals of LiF can be easily cleaved. The moisture can be attacked in the title crystal at 673 K and it will soften at 873 K. In view of the above-mentioned potential applications of this material, it is important to grow defect-free bulk single crystals. Most of the anisotropic physical properties of single crystals, such as optical, electrical and dielectric properties, deteriorate or are significantly diminished when they are not in the single-crystal domain or have defects such as structural grain boundaries (Bhagavannarayana, Ananthamurthy *et al.*, 2005; Bhagavannarayana, Budakoti *et al.*, 2005).

In the present work, a single crystal of LiF of 70 mm in length has been grown by an indigenously designed and developed Czochralski (CZ) crystal puller (Anantha Murthya *et al.*, 1993). In the CZ method, necking is one of the best techniques for achieving good quality crystals and hence we have used this technique in the present investigations. The crystalline perfection of the grown crystal was assessed at different regions along its growth direction with high-resolution X-ray diffraction (HRXRD). The optical transparency in the UV–vis region, photoluminescence (PL) and dielectric properties of samples chosen from different locations in the crystal boule with different degrees of crystalline perfection have been studied, and the observed correlation with the crystalline perfection has been discussed.

2. Experimental

2.1. Crystal growth

A CZ crystal puller designed, developed and fabricated at the National Physical Laboratory (NPL) was used. Fig. 1(*a*) shows a schematic of this system. Great care has been taken to ensure that the pulling motion is smooth and uniform. Two specially made stainless steel rods – one with a square cross section and surface planarity within 5 μm over its entire length of 1 m and another with a circular cross section – act as guides to the platform to which the seed is attached. The rate of pulling can be varied stepwise in the range 2–20 mm h^{-1}. The total available length of pulling is about 600 mm. A seed rotation assembly provides the desired rate of rotation to the crystal during growth. Special efforts have been made to isolate the furnace, the crucible, and the seed rotation and pulling assembly from vibrations generated in the system and in the surroundings. For this purpose, antivibration mountings of different types are used. The seed rotation assembly is driven by a 12 W synchronous motor. Particular attention was

paid to ensuring that the wobble around the rotation axis is negligible. In the experiments reported here, the rate of rotation was kept at 30 r min^{-1}. The LiF single crystal was grown using a platinum crucible of two inch (~5 cm) diameter. The temperature of the furnace was controlled using a Eurotherm temperature controller with an accuracy of ±0.1 K. The necking was performed at two places at different growth lengths. The grown bulk single crystal (shown in Fig. 1*b*) contains essentially five parts, the first one starting from the seed. The two necking places are between regions 1 and 2 and between regions 2 and 3; this phase was followed by a step growth by increasing the diameter between 3 and 4. Between 4 and 5, the diameter was increased and then a smooth and constant diameter was maintained. The required diameter control was achieved by slight temperature variations.

2.2. Characterization

The crystalline perfection of the grown single crystal in different regions was characterized by HRXRD by employing a multicrystal X-ray diffractometer developed at NPL (Lal & Bhagavannarayana, 1989). A well collimated and monochromated Mo $K\alpha_1$ beam obtained from three monochromator Si crystals set in a dispersive (+, −, −) configuration was used as the exploring X-ray beam. The specimen crystal was aligned in the (+, −, −, +) configuration. As a result of the dispersive configuration, though the lattice constants of the monochromator crystal(s) and the specimen are different, the unwanted dispersion broadening in the diffraction curve (DC) of the specimen crystal is insignificant. This arrangement improves the spectral purity ($\Delta\lambda/\lambda < 10^{-5}$)

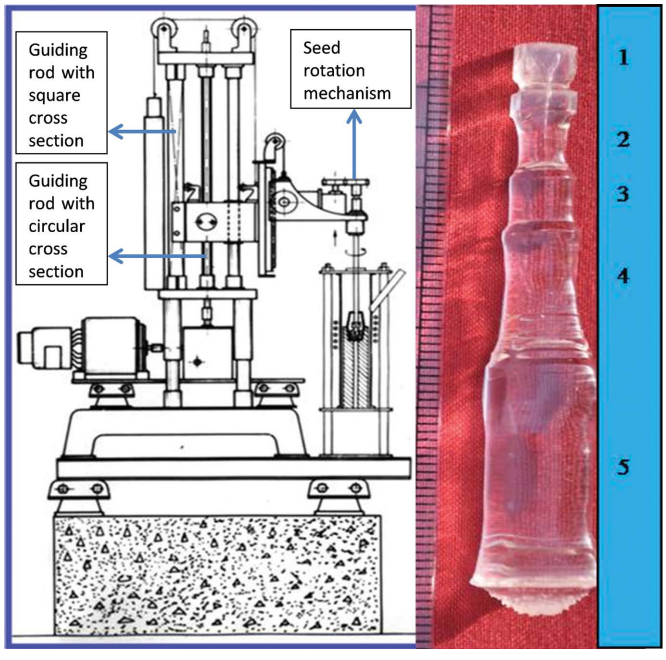

Figure 1
(*a*) Schematic of the home-made Czochralski crystal puller and (*b*) grown LiF single crystal.

of the Mo $K\alpha_1$ beam. The divergence of the exploring beam in the horizontal plane (plane of diffraction) was estimated to be $<<3''$. The specimen can be rotated about the vertical axis, which is perpendicular to the plane of diffraction, with a minimum angular interval of $0.4''$. The DC was recorded using the so-called ω scan method, wherein the detector was kept at the same angular position $2\theta_B$ [θ_B being the Bragg diffraction angle for the used diffracting planes, *i.e.* (200) for the LiF crystal, which is 10.15° for Mo $K\alpha_1$ radiation] with a wide opening for its slit. The voltage and current set for the X-ray source are 50 kV A and 30 mA, respectively. The size of the X-ray beam impinging on the surface is 5 × 0.2 mm with a stable beam intensity of 6.2×10^3 counts s^{-1}. The beam was allowed to fall at the center of the disc-shaped specimen during the experiments. Before choosing the central region, to confirm the homogeneity of the crystalline perfection, the diffraction curves were recorded across (diagonally) the sample at different places. However, except at the very edges, where some scattering is expected to occur for any sample, no appreciable variation either in the peak intensity or in the FWHM or in the asymmetry of the DC was observed. Five specimens with the same thickness (~2 mm) were cut normal to the growth direction from different regions of the grown crystal boule as indicated in Fig. 1. The cut surfaces were lapped and optically polished.

The optical absorption spectra of the specimens were recorded in the complete UV–vis region (200–1000 nm wavelength) using a Perkin Elmer Lambda-25 spectrophotometer.

The PL emission study was carried out by using a Perkin Elmer LS-55 fluorescence spectrofluorometer in the wavelength range 300–900 nm. The specimens were excited with a source of 200 nm.

To study the dielectric behavior, a PSM1735 impedance analyzer was used over the frequency range 50 kHz–15 MHz at room temperature. Silver paste electrodes were created on the parallel cut surfaces. Before being subjected to the analyzer, the specimens were dried at 373 K to remove moisture and paste diluter.

3. Results and discussion

3.1. High-resolution X-ray diffractometry analysis

The five crystal specimens were used to assess the crystalline perfection of the grown crystal at different regions along its growth direction. The HRXRD study revealed how the grain boundaries or dislocations that were initially present in the seed crystal were controlled with necking and step growth. Specimen 1 represents the used seed crystal, being taken from the region just above the start of the new crystal boule, and specimen 2 was taken from the part of the boule after the first necking at the seed but just before the second necking. Specimens 3–5 are taken from the middle portions of the parts labeled 3–5, respectively, in Fig. 1, which were grown with a stepwise increase of the diameter of the boule.

Figs. 2(*a*) and 2(*b*), respectively, show the diffraction curves recorded for specimens 1 and 2 in symmetrical Bragg geometry using Mo $K\alpha_1$ and the (200) diffracting planes. The diffracted intensity of these curves and the other DCs to be described are arbitrary, but the magnitude is relative. The experimental conditions, such as power and size of the X-ray beam, were the same and no normalization of either the peak area or the peak intensity was carried out. The (200) diffracting planes were used for recording the DCs for all the specimens. The range of the glancing angle for the DCs was chosen so as to cover the meaningful scattering intensity on both sides of the peak. The unit of glancing angle is arcseconds. On deconvolution of the diffraction curve shown in Fig. 2(*a*), it is clear that the curve contains two additional peaks, which are 648 and 412″ away from the main central peak. The solid red curve, which fits well with the experimental points (filled circles), was obtained by the convolution of the three peaks. Because of the good fit, it is clear that the two additional peaks correspond to two internal structural low-angle (tilt angle > 1 arcminute but less than a degree) grain boundaries (Bhagavannarayana, Ananthamurthy *et al.*, 2005) whose tilt angles (misorientation angle between the two crystalline regions on each side of the structural grain boundary) are 648 and 412″ from the main crystal block. The FWHM of the main peak and the very low angle boundaries are, respectively, 180, and 155 and 196″. Fig. 2(*b*) is recorded for specimen 2, which contains only one additional peak, and depicts a single low-angle boundary with a tilt angle of 192″. The FWHM of the main peak and the low-angle boundary are, respectively, 156 and 143″. The fact that the DC has a single low-angle boundary with a lower tilt angle, as well as the low FWHM values corresponding to the main crystal block and the low-angle boundary, reveal that the crystalline perfection of specimen 2 is much better than that of the seed-crystal specimen 1, showing that necking at the seed crystal helped to restrict the propagation of dislocations and grain boundaries into the growing crystal. However, it could not restrict the formation of a low-angle boundary. Fig. 3(*a*) shows the curve for specimen 3, grown after the necking. As seen in the figure, the DC contains a single sharp peak with a FWHM value of 78″, which is much less than those of the DCs in Figs. 2(*a*) and 2(*b*). These features clearly depict the substantial improvement of crystal quality as a result of necking.

It is interesting to see the asymmetry of the DC in Fig. 3(*a*). For a particular angular deviation ($\Delta\theta$) of glancing angle with respect to the peak position, the scattering intensity is much greater in the positive direction than in the negative direction. This feature clearly indicates that the crystal contains predominantly interstitial-type defects rather than vacancy defects. This can be well understood by the fact that, because of the presence of interstitial defects which may be due to fast

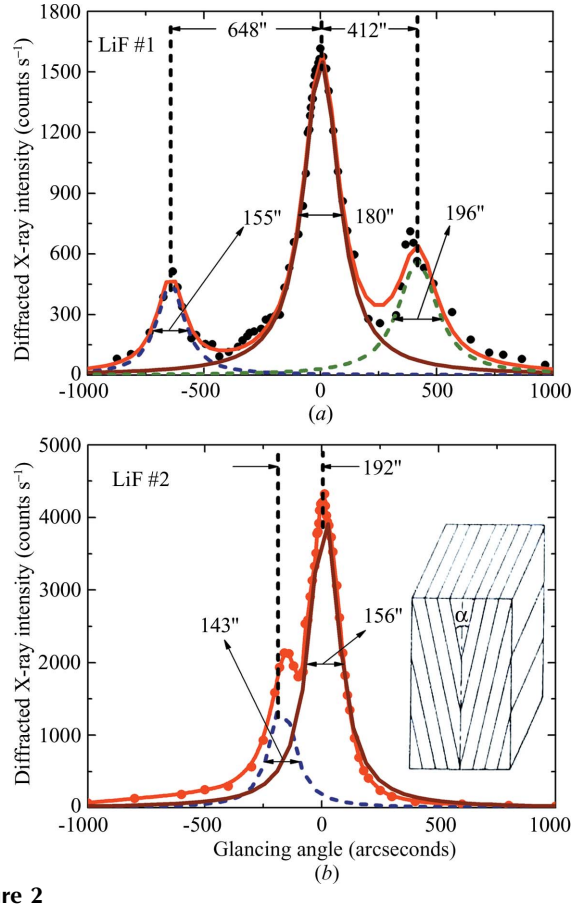

Figure 2
Diffraction curves recorded for specimens (*a*) 1 and (*b*) 2 using the (200) diffracting planes by employing the multicrystal X-ray diffractometer in symmetrical Bragg geometry.

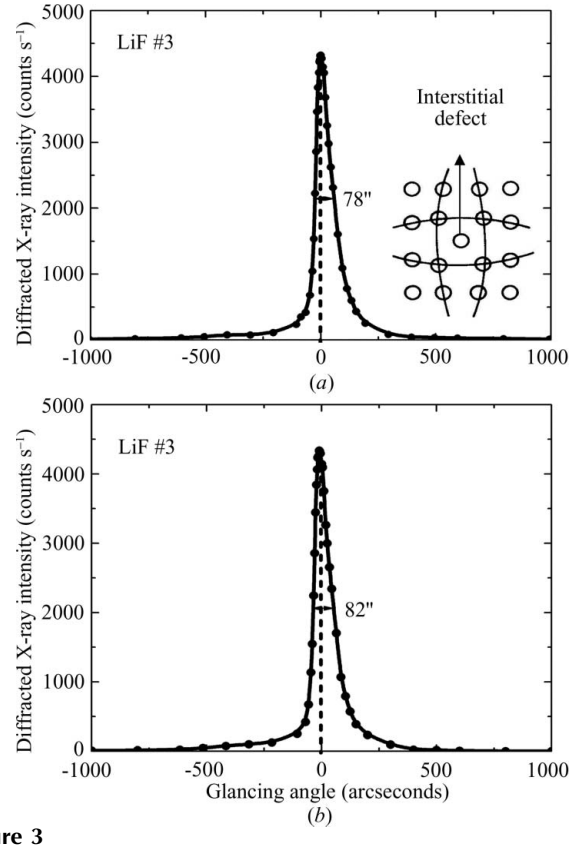

Figure 3
Diffraction curves recorded for specimen 3 using the (200) diffracting planes by employing the multicrystal X-ray diffractometer in symmetrical Bragg geometry. Curves (*a*) and (*b*) are for two in-plane positions with a 180° arc angular difference.

growth, the lattice around these defects undergoes compressive stress (Bhagavannarayana *et al.*, 2008) and the lattice parameter d (interplanar spacing) decreases [for the local portion of the crystallite around the defect core as depicted in the inset of Fig. 3(*a*)]. This leads to more scattering (also known as diffuse X-ray scattering) intensity at slightly higher glancing angles with respect to the exact Bragg angle (θ_B), as d and $\sin\theta_B$ are inversely proportional to each other in the Bragg equation ($2d\sin\theta_B = n\lambda$, n and λ being the order of reflection and wavelength, respectively, which are fixed). However, the single sharp diffraction curve with reasonably low FWHM indicates that the crystalline perfection is fairly good. The density of such interstitial defects is, however, very low. In almost all real crystals, including crystals formed by natural geological processes, such defects are commonly observed and often are unavoidable owing to thermodynamical conditions and hardly affect the device performance. More details may be obtained using high-resolution diffuse X-ray scattering measurements (Bhagavannarayana, Budakoti *et al.*, 2005), but this is not the main focus of the present investigation. It is worth mentioning here that the observed scattering due to interstitial defects is of short-range order, as the strain due to such minute defects is limited to the core of the defect and long-range order could not be expected. Quantitative determination of the minute change in d value (whose fractional change $\Delta d/d = -\Delta\theta\cot\theta_B$ is expected to be in the range from 10^{-4} to 10^{-6} when $\Delta\theta$ is in arcseconds as in the present case) confined to a very localized region around the defect core is not an easy task, but the effect of this change can be seen from the observed scattering intensity along the tails of the rocking curve (RC), as in the present study. Actually, the lattice constants determined by the X-ray diffraction technique depend upon the peak position. However, the peak position is hardly changed by the scattering intensity due to point defects because the associated strain is limited to the defect core, as mentioned above. Thus, such defects do not cause any change in the lattice parameters of the crystal. Porous silicon (PS) is a good example in which the surface, which contains pores distributed homogeneously with high density and up to a good depth (of the order of micrometres), acts as if it has a larger lattice constant. As a result of this enlargement of the lattice constant ($\Delta d/d \simeq 10^{-4}$) by the tensile strain in the PS strands (chemically attached to the silicon substrate) surrounding the pores, the diffraction curve contains an additional resolved peak (Bhagavannarayana *et al.*, 2006). Further changes in $\Delta d/d$ due to adsorption of suitable gases in the pores could also be measured quantitatively by the change in the separation of the diffraction peaks due to the PS film and the Si substrate (Sharma *et al.*, 2007). However, as explained above, the localized strain developed by point defects with low density (of the order of parts per million) could not produce any additional peak in the diffraction curve. Such minute localized structural changes may be seen by the use of high-resolution transmission electron microscopy. However, the sample preparation is rather tedious, and because of the presence of artefacts one cannot really detect the actual d-parameter changes. It may also be mentioned here that, even in doped crystals, wherein the dopants occupy the interstitial sites, no change in the overall lattice parameter could be found by standard powder X-ray diffraction analysis (wherein the positions of many peaks are taken into account for lattice-parameter determination through various refinement processes), as again the strain developed by such defects is very localized and could not change the overall lattice parameter (Kushwaha *et al.*, 2010; Bhagavannarayana *et al.*, 2008). However, while attributing the asymmetry of an RC to point defects, doubts may arise as to whether the observed asymmetry is due to the probable mosaicity of the crystal; in this case the micro- or nano-sized crystallites or mosaic blocks may have a preferred orientation (if they are oriented randomly, one cannot get any asymmetry), which could be misoriented by only a few arcseconds from the main crystal block. If the misorientation angle between the preferred orientation angle and the exact normal to the crystallographic planes of the main crystalline block is higher, one would expect a very broad FWHM or additional peak(s) as in the RCs of Figs. 2(*a*) and 2(*b*). To resolve this doubt, an additional RC was recorded after rotating the crystal by 180° in-plane (Fig. 3*b*) under identical conditions to those of Fig. 3(*a*). However, as seen in the figure the same type of asymmetry in the RC was found, with little difference in the value of FWHM, which is within the experimental uncertainties. If there is a preferred orientation, the asymmetries in the RCs would be expected to be opposite to each other in Figs. 3(*a*) and 3(*b*), with mirror symmetry. From this it is clear that the observed asymmetry is due to point defects and/or their aggregates (Lal & Bhagavannarayana, 1989). Such asymmetry could be observed very prominently in heavily doped single crystals (Bhagavannarayana *et al.*, 2008). The FWHM values of the RCs in Fig. 3 are somewhat higher than that expected from the plane wave theory of dynamical X-ray diffraction (Batterman & Cole, 1964) for an ideally perfect crystal but close to that expected for nearly perfect real crystals. Theoretical details of the DC and FWHM are described in the following.

In the case of symmetrical (the diffracting planes are parallel to the surface) Bragg reflection one can obtain the following equation for the reflection coefficient [ratio of the diffracted beam intensity (I_d) to the intensity of the incident beam (I_0)]:

$$(I_d/I_0)_{\mu\neq 0} = |\eta \pm (\eta^2 - 1)^{1/2}|^2. \quad (1)$$

Here $\eta = \eta' + i\eta''$ is an important parameter related to the glancing angle θ, structure factor and wavelength of the X-ray beam as given below:

$$\eta' = \left(\frac{-\Delta\theta\sin 2\theta + \tau F_0'}{|P|\tau F_H'}\right) \quad \text{and} \quad \eta'' = \left(\frac{F_H''}{F_H'}\right)\left(\eta' - \frac{1}{|P|\varepsilon}\right), \quad (2)$$

where $\Delta\theta$ is the relative glancing angle with respect to the peak position, $\tau = r_e\lambda^2/\pi V$, r_e is the classical electron radius, V is the volume of the unit cell, P is the polarization factor, F_H' and F_H'' are the real and imaginary components of the structure

factor for the *hkl* reflection given by $F_H = F'_H + F''_H$, and ε is the ratio of the imaginary part F''_H to F''_0, which can be calculated as $F''_0 = \mu_0\lambda/2\pi\tau$, μ_0 being the linear absorption coefficient. The effect of thermal motion of atoms in the crystal at finite temperature is included through the Debye–Waller factor for the structure factor in the above equation. The specification $\mu \neq 0$ in the above equation implies that the absorption of X-rays is also taken care of. Fig. 4 shows the theoretical diffraction curve using the (200) diffracting planes of an LiF single crystal and Mo $K\alpha_1$ radiation. For the sake of convenience, the x axis is drawn in terms of glancing angle θ. As the X-ray beam is parallel, monochromatic and plane polarized because of successive diffraction from the three monochromators, the factor P is taken as unity. The FWHM ($\Delta\theta_{1/2}$) of such a curve can be readily obtained from the following simplified equation:

$$\Delta\theta_{1/2} = \frac{2\tau}{\sin 2\theta_B} F'_H |P|. \qquad (3)$$

Fig. 4 in fact contains two diffraction curves: one the so-called Darwin, where the phenomenon of linear absorption of X-rays is not taken into consideration, and the other the well known Darwin–Prince curve, in which the absorption correction is taken into account. From Fig. 4 it is observed that (i) the reflectivity at the peak of the diffraction maximum is nearly 100%, even in the Darwin–Prince curve, and (ii) the intensity of the diffracted X-ray beam is appreciable only in a very narrow angular range, with half-width of only 0.57″. The high reflectivity and very low FWHM for the DC are expected because of the very light elements (the lower the atomic number, the lower the atomic scattering factor) that constitute the LiF crystal; for example, in contrast, the FWHM is ∼9.5″ for CdTe. The departure from the ideal state of atomic arrangement in the specimen will be seen as the difference between the half-widths and the peak reflectivities of the two curves. Of course, the experimental arrangement for recording diffraction curves should be such that the exploring X-ray beams are nearly parallel and monochromatic. The lowest FWHM that has been observed so far with the present diffractometer is 2.7″ for an excellent quality potassium dihydrogen phosphate single crystal (Dhanaraj *et al.*, 2009), with which one can realize the resolution of the diffractometer.

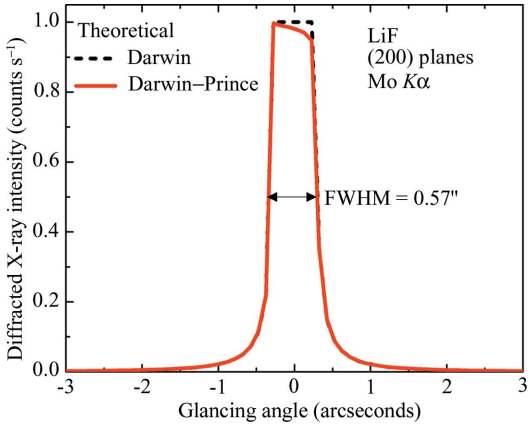

Figure 4
Theoretical diffraction curve for the (200) diffracting planes using Mo $K\alpha_1$ radiation for an ideally perfect LiF single crystal using the plane wave dynamical theory of X-ray diffraction.

It may be mentioned here that observing detailed information like the asymmetry in the DC is possible in the present sample only because of the high resolution of the multicrystal X-ray diffractometer used in the present investigation. Fig. 5(*a*) shows the DC recorded for specimen 4. As seen in Fig. 5(*a*), the FWHM is 60″, which is considerably lower than those in Figs. 3(*a*) and 3(*b*), showing that the step growth also helped significantly in improving the crystalline perfection. The nature of the asymmetry and hence the type of point defects (interstitials) is the same as that of specimen 3 in Fig. 3. Fig. 5(*b*) shows the DC corresponding to specimen 5. This DC is also more or less similar to those of Figs. 3(*a*) and 3(*b*), but there is a slight difference in the asymmetry. In this curve the scattering intensity is relatively more on the negative side with respect to the peak position, showing that this specimen contains predominantly vacancy-type point defects. This may be due to Li vacancies created by the evaporation of Li during the prolonged heating of the material at elevated temperature, as supported by the PL studies (§3.3).

3.2. UV–vis absorption study

The recorded UV–vis absorption spectra for specimens 3, 4 and 5 (which are free from structural grain boundaries) are

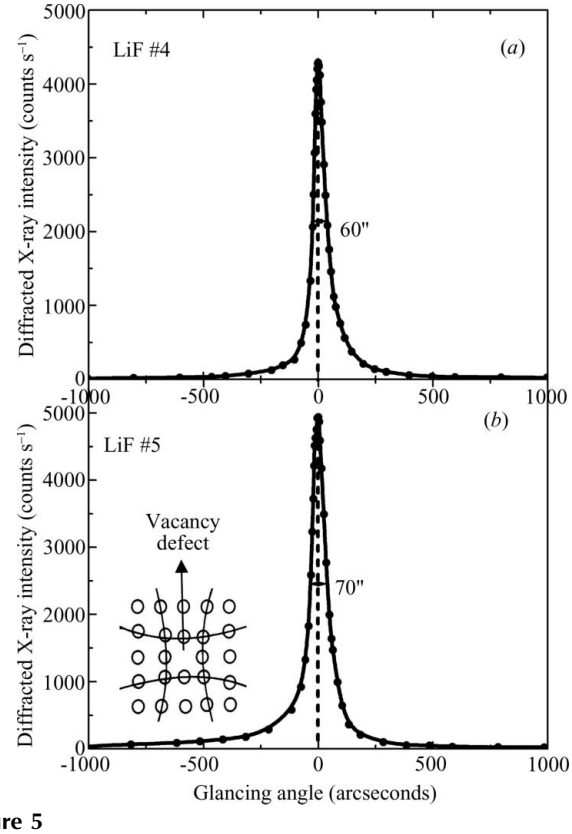

Figure 5
Diffraction curves recorded for specimens (*a*) 4 and (*b*) 5 using the (200) diffracting planes by employing the multicrystal X-ray diffractometer in symmetrical geometry using Mo $K\alpha_1$ radiation.

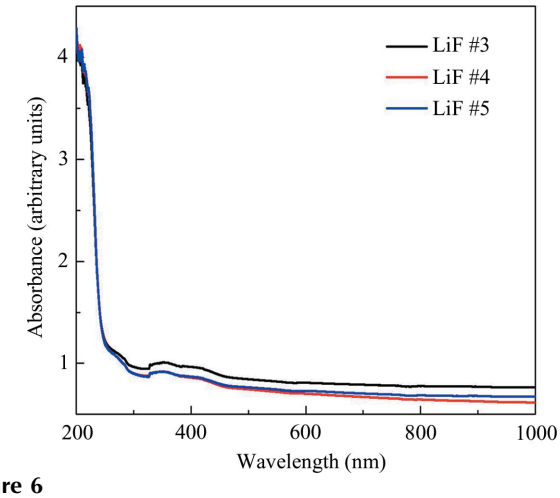

Figure 6
UV–vis absorption spectra of specimens 3–5 of the LiF single crystal.

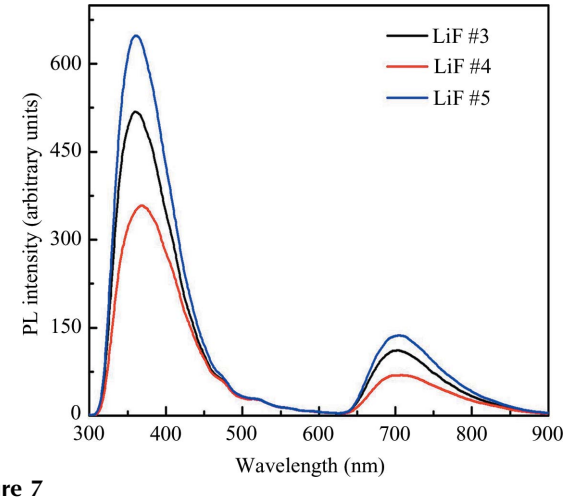

Figure 7
PL spectra of specimens 3–5 of the LiF single crystal.

shown in Fig. 6. From the spectra it is clear that the crystal is quite transparent over the entire UV–vis spectrum. Specimen 3 has slightly less transparency over the entire spectrum, which may be due to the excess interstitial defects. For specimen 4 whose FWHM is least, the transparency is maximum. For specimen 5, maybe because of the Li^+ vacancies generated during the prolonged heating of the charge, the transparency has been slightly reduced.

3.3. Photoluminescence analysis

The photoluminescence emission spectra for specimens 3, 4 and 5 are shown Fig. 7. As seen in the figure, the PL is less in the more perfect region (4) and maximum in specimen 5. The latter contains predominantly the vacancy defects that may be due to the presence of more Li^+ vacancies, which act as color centers thus leading to higher PL intensity.

3.4. Dielectric analysis

A log–log plot of relative dielectric constant (ε_r) with frequency (Fig. 8*a*) for all the specimens shows that the ε_r

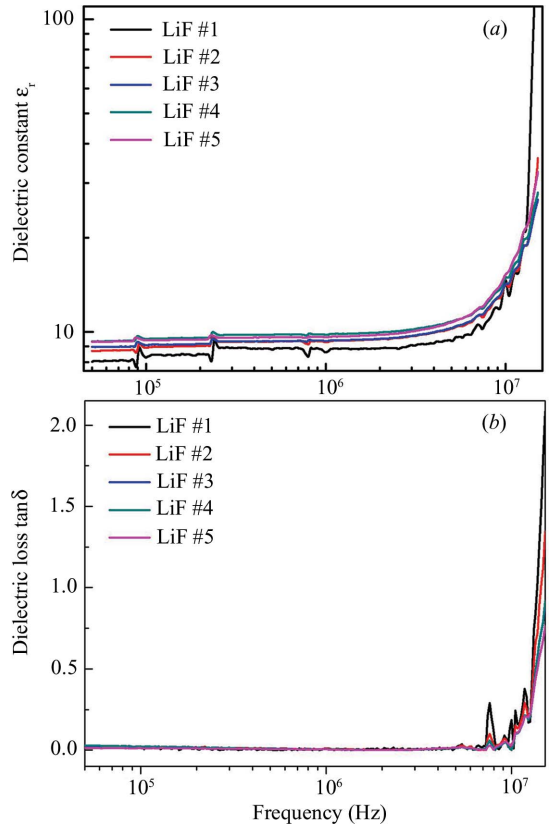

Figure 8
(*a*) Dielectric constant and (*b*) dielectric loss of specimens 1–5 of the LiF single crystal.

values up to 5 MHz are almost constant and less than 10. Above this frequency, the ε_r values increase sharply, and specimen 1 with structural grain boundaries attains the maximum value among the specimens, whereas at lower frequencies sample 1 has the minimum value. The dissipation factors ($\tan\delta$) as seen in Fig. 8(*b*) for all the specimens are almost zero for frequencies up to 10 MHz, and above this frequency they sharply increase. Except for specimen 1 with grain boundaries, all the curves are smooth, which shows that the grown crystal can be efficiently used for dielectric applications over a wide range of frequencies.

4. Conclusions

From the above studies it is demonstrated that necking and subsequent step growth in LiF crystals is very useful for growing good quality crystals. The observed correlation of the investigated physical properties of optical transparency, photoluminescence and dielectric properties with the crystalline perfection is discussed.

The authors are grateful to the Director, NPL, for continuous encouragement for crystal growth and crystallography activity at NPL. The authors are also thankful to Dr D. Harnath for carrying out PL studies. SKK is thankful to CSIR, India, for providing an SRF fellowship.

References

Anantha Murthya, R. V., Bartwala, K. S. & Lal, K. (1993). *Mater. Sci. Eng. B*, **18**, L4–L6.

Basiev, T. T., Zverev, P. G., Papashvili, A. G. & Fedorov, V. V. (1997). *Kvantovaya Elektronika* (*Moscow*), **27**, 574–578.

Batterman, B. W. & Cole, H. (1964). *Rev. Mod. Phys.* **36**, 681–717.

Bhagavannarayana, G., Ananthamurthy, R. V., Budakoti, G. C., Kumar, B. & Bartwal, K. S. (2005). *J. Appl. Cryst.* **38**, 768–771.

Bhagavannarayana, G., Budakoti, G. C., Maurya, K. K. & Kumar, B. (2005). *J. Cryst. Growth.* **282**, 394–401.

Bhagavannarayana, G., Parthiban, S. & Meenakshisundaram, S. (2008). *Cryst. Growth Des.* **8**, 446–451.

Bhagavannarayana, G., Shailesh Sharma, N., Sharma, R. K. & Lakshmikumar, S. T. (2006). *Mater. Chem. Phys.* **97**, 442–447.

Dergachev, A. Yu. & Mirov, S. B. (1998). *Opt. Commun.* **145**, 107–112.

Dhanaraj, P. V., Rajesh, N. P., Mahadevan, C. K. & Bhagavannarayana, G. (2009). *Physica B*, **404**, 2503–2508.

Kushwaha, S. K., Shakir, Mohd., Maurya, K. K., Shah, A. L., Wahab, M. A. & Bhagavannarayana, G. (2010). *J. Appl. Phys.* **108**, 033506.

Lal, K. & Bhagavannarayana, G. (1989). *J. Appl. Cryst.* **22**, 209–215.

Numan Salah, S. P. D. & Rupasov, A. A. (2007). *J. Lumin.* **124**, 357–364.

Sharma, S. N., Bhagavannarayana, G., Umesh Kumar, Debnath, R. & Chandra Mohan, S. (2007). *Physica E*, **36**, 65–72.